https://doi.org/10.5194/nhess-2022-178
Preprint. Discussion started: 6 July 2022

Natural Hazards and Earth System Sciences
Discussions
Open Access
EGU

Analysis of the relationship between yield in cereals and remotely sensed fAPAR in the framework of monitoring drought impacts in Europe

Carmelo Cammalleri, Niall McCormick, Andrea Toreti
European Commission, Joint Research Centre (JRC), 21027 Ispra (VA), Italy.
Correspondence to: Carmelo Cammalleri (carmelo.cammalleri@ec.europa.eu)

Abstract. This study analyses the relationship between satellite-measured fAPAR (Fraction of Absorbed Photosynthetically Active Radiation), which are continuously monitored by the European Drought Observatory (EDO) of the EU's Copernicus Emergency Management Service, and crop yield data for cereals, which are collected by Eurostat. Different features of the relationship between annual yield and multiple time series of fAPAR, collected during different periods of the year, were investigated. Two key outcomes of the analysis were the identification of the period from March to October as that when the highest positive correlation between fAPAR and yield is detected in Europe on average, and February to May as the period when most of the negative correlation are observed. While both periods align well with the commonly assumed dynamic of the growing season, spatial differences are also observed across Europe. On the one hand, the Mediterranean regions report the highest correlation values ($r > 0.8$) and the longest continuous periods with positive statistically significant results (up to 7 months), covering most of the growing season. On the other hand, the central European region is characterized by the most limited positive correlation values, with only 2 months or less showing statistically significant results. While marked differences on the overall capability to capture the full dynamic of yield are observed across Europe, fAPAR anomalies seem capable to distinguish between drought and no/drought years in most of the cases if negative yield anomalies are used as a proxy variable for drought impacts.

Keywords: vegetation indices, agricultural drought, EDO, CEMS.

https://doi.org/10.5194/nhess-2022-178
Preprint. Discussion started: 6 July 2022


Natural Hazards and Earth System Sciences
Discussions

1. Introduction

Drought is a multifaceted phenomenon threatening societies, economies and ecosystems in a complex web of cascading effects (UNDRR, 2021). Amongst the major sectors that are impacted by drought, agriculture is still recognized as the most sensitive one (FAO, 2015; FAO et al., 2018), as reflected by the large share of reported impacts for agriculture over the majority of countries and drought events in Europe (Stahl et al., 2016).

Most drought monitoring systems recognize the prominent role of agricultural drought, by refining indicators of meteorological drought in order to better account for impacts on vegetation growth (e.g. the Standardized Precipitation-Evapotranspiration Index – or SPEI; Vicente-Serrano et al., 2012), and/or by directly incorporating drought indicators that are based on remotely sensed vegetation indices (WMO and GWP, 2016). In particular, negative deviations from climatological values of satellite measurements of vegetation "greenness" – for example, the standardized anomalies of the fraction of Absorbed Photosynthetically Active Radiation (fAPAR) that are provided by the European and Global Drought Observatories (EDO and GDO, https://edo.jrc.ec.europa.eu) – are often adopted as a proxy variable for the adverse effects of drought on vegetation.

While such approaches are logically based on the connection between reduced vegetation greenness and diminished plant productivity, it is also well known that droughts occurring during different phenological stages may have different impacts on yield and production (i.e. Barros et al., 2021; Ceglar et al., 2020; Chaves et al., 2002; Demirevska et al., 2009; Stallmann et al., 2020; Zampieri et al., 2017). Consequently, greenness anomalies can be interpreted differently, depending on the development stages of the vegetative cycle when they manifest. Some studies have tried to account for this concept by limiting the analysis to the growing period and excluding data for the plant dormancy phase (e.g. Rojas et al., 2011), by deriving key variation metrics (i.e. amplitude, integral, maximum) from the full growing season (e.g. Kang et al., 2018), or by focusing only on key periods (i.e. a specific month) that have been shown to correlate well with deviations in annual yield for a given study area (Bachmair et al., 2018).

Within the framework of the near real-time monitoring of drought events, the task of evaluating and quantifying the actual relevance of an observed anomaly in vegetation greenness is complicated by the need to update continuously the status based on newly acquired data, without the benefit of the full picture of the complete vegetation cycle. This limits the possibility to implement some of the above mentioned approaches as part of

https://doi.org/10.5194/nhess-2022-178
Preprint. Discussion started: 6 July 2022

operational drought monitoring systems, other than the simple masking of data acquired outside of a pre-defined growing season. An example of an early warning system that accounts for the timing of the observed anomalies is the Anomaly Hot Spots of Agricultural Production (ASAP) decision support system (Rembold et al., 2019), where the seasonal progression (expansion, maturity, senescence) is explicitly considered in determining the warning level.

As part of the shift in the drought risk management paradigm from a reactive to a proactive approach, the move from simple hazard indicators to quantitative assessments of risk and impacts is likely to be further integrated within modern early warning systems (UNDRR, 2021). In this regard, independent estimates of actual drought impacts, such as records of yield deviations for different crop types, constitute a valuable reference to assess how the relationship between anomalies in vegetation indices and drought conditions varies in space and throughout the year. This also enables the evaluation of the efficiency of remotely sensed indicators as a proxy for the effect of drought on vegetated land, and the refinement of their use as stress-forcing data for agro-economic models, for the assessment of losses in agriculture due to droughts (García-León et al., 2021).

In this context, the primary goal of this study is to analyse to what extent the year-by-year dynamics of yield in Europe can be explained by a regularly updated operational drought indicator, in particular by the fAPAR anomalies produced by EDO. Yield data for cereals, recorded by Eurostat, are used as a general proxy for the impact of droughts on agriculture. The spatio-temporal variations in the relationship between dekadal (i.e. 10-day) fAPAR anomalies and yearly yield deviations can help in identifying the periods of the year when these two quantities are most closely related in the different parts of Europe, thus providing a quantitative basis for improving the assessment of drought impacts in agriculture, with potential benefits both for drought monitoring systems and for agro-economic models in Europe.

2. Material and Methods

2.1 Eurostat yield dataset

Eurostat, the European Statistical Office, publishes regular reports of statistics on annual crops, including data on production, cultivated area and yield for different crop types, at both national and sub-national aggregation levels (Eurostat, 2020), with the aim of providing a harmonized database of data collected by EU Member States and neighbouring countries.

https://doi.org/10.5194/nhess-2022-178
Preprint. Discussion started: 6 July 2022


Natural Hazards and Earth System Sciences
Discussions

For the purposes of this study, annual data on yield for cereals have been retrieved between 2001 (first full year with available fAPAR data) and 2018 (last available year in the Eurostat database at the time of this study), mostly at the spatial scale of Eurostat's so-called "NUTS 2" regions (hereafter referred to simply as regions). Only in the case of Germany and the UK data at the NUTS 1 level were used, in order to maximize both data coverage and consistency in region size with the rest of the domain.

Because the yield data are to be used for computation of deviations from the long-term average, temporal consistency in the data records is essential. For this reason, records that are flagged by Eurostat as estimated, provisional, unreliable or with a definition that differs due to missing components, were excluded from the analysis.

Systematic changes in the annual yield time series were removed by applying a Savitzky–Golay filter to account for advancement in technology and crop management (Tadesse et al., 2015), before standardized anomalies were computed only for those regions with more than 9 years of data (i.e. half of the analyzed period). In this way, 240 regions with valid time series were obtained.

2.2 MODIS fAPAR dataset

The fraction of Absorbed Photosynthetically Active Radiation (fAPAR) is one of the 50 Essential Climate Variables recognized by the UN Global Climate Observing System (GCOS), mainly thanks to its direct relationship with primary production (https://gcos.wmo.int/en/essential-climate-variables/fapar).

fAPAR, and in particular its deviations from historical climatology, constitutes the ideal proxy variable for the effects of drought on vegetated lands (Rossi et al., 2008). In this context, remote sensing images collected by the MODIS (MODerate resolution Imaging Spectroradiometer) sensor represent a unique data source for drought studies, due to the unprecedented longevity of the Terra satellite.

In this study, the standard MODIS Terra LAI/fAPAR product (i.e. MOD15A2H, Collection 6) is used (Myneni, 2015), in which global fAPAR maps are derived from the atmospherically corrected Bidirectional Reflectance Distribution Function (BRDF) recorded by MODIS in 7 spectral bands, by solving the three-dimensional radiation transfer process through a look-up-table approach (Knyazikhin et al., 1998; Wang et al., 2001).

The standard MODIS product is distributed as 8-day composites (using a maximum composite method) at a spatial resolution of 500-m in 1,200 × 1,200 km tiles on a sinusoidal

https://doi.org/10.5194/nhess-2022-178
Preprint. Discussion started: 6 July 2022


Natural Hazards and Earth System Sciences
Discussions

grid. Data include a quality assessment (QA) layer that allows to detect where the simplified back-up algorithm has been used.

Datasets of both fAPAR and fAPAR anomalies based on MOD15A2H raw data are regularly produced as part of the European and Global Drought Observatories (EDO and GDO, https://edo.jrc.ec.europa.eu) of the EU's Copernicus Emergency Management Service. The operational fAPAR dataset is obtained after a set of pre-processing procedures, including: 1) screening of the low-quality data based on the QA flag; 2) spatial aggregation of the data (simple average) at 1-km resolution and re-projection onto a lat/lon regular grid at 0.01° resolution with nearest neighbour resampling; 3) temporal aggregation at dekadal scale (three maps per month: days 1–10, 11–20 and 21–end-of-month) by means of a weighted average of the two closest 8-day images (weight proportional to the overlapping with the dekadal period); and 4) exponential temporal smoothing of the dekadal data (with smoothing parameter equal to 0.5; Brown and Meyer, 1961).

Here, the fAPAR anomalies were computed as standardized deviations from the reference period (2001-2018), only if at least 6 years of data were available and only where the long term standard deviation was greater than 0.01 (to exclude areas of low variability, such as deserts or highly stable densely vegetated areas). The reference period of 2001-2018 is consistent with the one used for the yield anomalies.

2.3 Analysis strategy

In this study, the analysis of the relationship between the dekad time series of fAPAR anomalies and yearly crop yield is based primarily on computation of the Spearman correlation coefficient (r). In order to carry out the analysis, the two main discrepancies between the two datasets, namely regarding the spatial units (i.e. regions versus cells) and temporal frequency (year versus dekad), must first be considered.

Given the focus of the study, the only fAPAR conditions that are relevant are the ones observed over arable land. Therefore, the fAPAR anomaly data were first upscaled to NUTS 2 regions as a weighted average of all the 0.01° resolution fAPAR anomaly values within a region, with a weighting factor based on the fraction of each grid-cell classified as arable land according to the latest Corine land cover map (CLC2018, https://land.copernicus.eu/pan-european/corine-land-cover/clc2018).

Regarding temporal frequency, while fAPAR anomaly data are available throughout the year, similar studies (e.g. Rojas et al., 2011) have focused only on data collected during the growing season. A north-to-south gradient have been observed in the start, the end, and the

https://doi.org/10.5194/nhess-2022-178
Preprint. Discussion started: 6 July 2022


Natural Hazards and Earth System Sciences
Discussions

length of the growing season in Europe, with April-September being a common period all over Europe, but with early start in February and late end in November over many areas (Rötzer and Chmielewski, 2001). Estimations of the growing season directly based on remotely sensed vegetation indices have also highlighted a very early start in the Mediterranean, around October/November of the previous year (i.e., Atzberger et al., 2014), likely related to the effect of infesting weeds on the remote sensing signal. Following these considerations, here we analyse an extended period, testing the relationship between the yield of a particular year and the fAPAR anomalies between the first dekad of October of the preceding year and the end of the current year, for a total of 45 dekadal time series.

The set of correlation analyses between each of the 45 dekadal time series of fAPAR anomalies and yearly yield data is used to construct a "correlogram", which relates the dekad with the corresponding r value (see example in Fig. 1 for the Tuscany region in Italy). Different analyses can be performed on the correlograms, depending on the critical values that are extracted from these plots and on the goal of the analysis. Here, we faced the problem in two different ways: a) detecting periods of similar behaviour and accuracy but variable length; and b) detecting periods of similar length but variable accuracy and behaviour.

For these two analyses, we distinguished between two different behaviours in the fAPAR-yield relationship, a direct relationship (i.e. negative anomalies in fAPAR correspond to negative anomalies in yield) and an inverse relationship. The latter may occur when a strong vegetative growth in observed early in the season during drought years, especially in energy-limited conditions (van Hateren et al., 2021). We also distinguished between two levels of accuracy, statistically significant correlations ($p < 0.05$, either positive or negative) and at least different than zero r values (i.e. $|r| > 0.15$).

Starting with a minimum length of 2 dekads, up to 990 periods of various length (L, from 2 up to 45 dekads) can be analyzed for each region, and for each of these periods four main metrics are computed: 1) F_{p+}, the fraction of r values in the period that are positive and statistically significant (i.e. $r > 0$ and $p < 0.05$; 2) F_{p-}, the fraction of r values in the period that are negative and statistically significant (i.e. $r < 0$ and $p < 0.05$); 3) F_{+}, the fraction of r values in the period that are at least positive (i.e. $r > 0.15$), and 4) F_{-}, the fraction of r values in the period that are at least negative (i.e. $r < -0.15$). We can then focus on the longest periods that have homogeneous behaviour and accuracy for a given region, namely homogeneous periods from hereafter (i.e. a period with $F_{p+} = 1$ represents a continuous streak of dekads with all positive and statistical significant r values). In the example reported in Figure 1, the dekads between 23 and 36 (light grey area) are clearly part of the longest period with all positive and

https://doi.org/10.5194/nhess-2022-178
Preprint. Discussion started: 6 July 2022

193 statistically significant r values, L = 14, while the dark grey area demarks the longest period
194 with F_{-} = 1 (L = 6).
195 A further set of analyses is focused on a fixed time window, or a limited range of
196 lengths, which boundary values can be derived from the previous tests. Within these limits, an
197 optimal positive (negative) period for each region can be defined as the period with the
198 maximum (minimum) average r value. Differently from the first group of analyses, these
199 optimal periods have varying F_{p+} and F_{+} (F_{p+} and F_{+}) values that can be used to quantify the
200 robustness of the relationship between fAPAR and yield.
201 Finally, while the analyses based on correlation give an insight on the relationship
202 between fAPAR and yield over the full spectrum of variability, a further test focused only on
203 drought conditions is also performed, given that in the context of drought monitoring it would
204 be sufficient to be able to distinguish drought-affected years from the rest. Here, the total
205 number of cells for each region with fAPAR anomalies < -1 is computed during the drought
206 years (yield anomalies < -1), and it is compared with the same during no-drought years (yield
207 anomalies ≥ -1). The assumption here is that the ratio of these two quantities should be greater
208 than one in the case of a direct relationship.

209 **3. Results and Discussion**

210 **3.1 Yield anomalies as a proxy variable for drought impacts**

211 Since standardized yield anomalies for cereals, as described in Section 2.1, are here used as a
212 proxy variable for the effects of droughts on vegetated land, a preliminary analysis was
213 performed to evaluate the reliability of this assumption for the derived dataset.
214 Figure 2 depicts the temporal evolution of yearly yield deviations, highlighting some
215 clear spatial patterns of significantly negative anomalies (i.e. yield anomaly < -1). Following a
216 review of the scientific literature for past drought events, it is possible to associate a
217 documented main drought event to each of these large clusters, as summarized in Table 1.
218 Seven main droughts are reported, ranging from the well-known drought in central Europe of
219 2003 (Rebetez et al., 2006) to the central-north European drought of 2018 (Buras et al., 2020;
220 Toreti et al., 2019).
221 The existence of a cause-effect relationship between the largest spatial patterns
222 observed in negative yield anomalies and the listed major drought events is further supported
223 by the study of Spinoni et al. (2015), which categorized the listed events (except the last two,
224 which occurred after that study) as being among the most severe in Europe according to
225 meteorological drought indices.

https://doi.org/10.5194/nhess-2022-178
Preprint. Discussion started: 6 July 2022


Natural Hazards and Earth System Sciences
Discussions

For each of the drought events listed in Table 1, specific independent scientific references are also provided, which include details on the evolution of the meteorological conditions, and the potential impacts on agriculture. Overall, analyses of these data tend to support the underlying assumption that yield anomalies can be used as a reliable independent estimate of drought impacts on vegetation, in conformance with the conclusions of other studies at regional level in Europe (Bachmair et al., 2018; Potopová et al., 2015), or for other parts of the world (e.g. Yang et al., 2020).

3.2 Detection of the homogeneous periods in the fAPAR-yield relationship

While many studies focused on the local maximum *r* value to detect when and where fAPAR and annual yield anomalies best correlate, isolated peak values may alter the perception of the robustness of fAPAR as a proxy variable of yield. In the context of an operational drought monitoring system, where continuous estimates should be provided rather than "one shot" predictions, information on longer homogeneous time periods are more valuable.

Focusing first on the positive *r* values, we analysed the periods with only statistically significant values (F_{p+} = 1), or only at least positive values (F_{+} = 1). The maps in Fig. 3 reports the local maximum lengths corresponding to these two quantities, namely positive homogeneous periods. Both of these maps show generally longer homogeneous periods in southern Europe, with the largest values observed for some Mediterranean regions (e.g. most of Spain, Cyprus, Sicily, Apulia and the Aegean/Mediterranean Turkey), and the smallest values (or no homogeneous period at all) mostly located in Central Europe (i.e. Germany, Poland and north-eastern France). On average, the maximum length of the periods with F_{p+} =1 is limited in most of the cases (5.5 ± 4.3 dek, almost 2 months), whereas the values more than double in the case of F_{+} = 1 (13.0 ± 8.3 dek, more than 4 months).

Generally, almost all the maximum *r* values in the correlograms are obtained in the dekads between mid-February and mid-September, which is expected since this period aligns well with what is commonly considered the growing season in Europe (Atzberger et al., 2014; Rötzer and Chmielewski, 2001). Nonetheless, a large variability in the length of both positive homogeneous periods is observed, with southern and central Europe confirmed to be not only the areas with highest and lowest *r* values, respectively, but also the areas with the longest (i.e. 4-7 months) and shortest (up to 2 months) periods with consecutive statistically significant positive correlations.

https://doi.org/10.5194/nhess-2022-178
Preprint. Discussion started: 6 July 2022

In order to evaluate synthetically the temporal location of these homogeneous periods, we analyzed which dekads each of them covers, and computed for every dekad the fraction of NUTS 2 regions (out of 240) that includes that particular dekad in the homogeneous period (Fig. 4). For example, dekad 27 (i.e. the first dekad of July starting from the beginning of October of the previous year) is part of the maximum homogeneous period in about 20% and 50% of the regions, for F_{p+} and F_{+}, respectively. It is worth noting that about 21% of the NUTS 2 regions do not have a period (minimum 2 consecutive dekads) with $F_{p+} = 1$.

It is possible to observed two "flexing points" in each of the two time series in Fig. 4: both around the values 0.1 for F_{p+} and around 0.2 for F_{+}. Starting from these values, we can detect two optimal homogeneous periods: from end-of-April to mid-October (6 months) for F_{p+}, and from March to early-November (8 months) for F_{+}.

Moving to the negative correlation values, two maps analogous to the ones in Fig. 3 are reported in Fig. 5 for F_{p-} (panel a) and F_{-} (panel b). These two maps show how the longest negative homogeneous periods are in general shorter than the ones for positive correlations, with an average value of 3.0 ± 1.6 dekads for F_{p-} and 7.0 ± 3.9 for F_{-}. The lack of statistically significant negative r values is especially evident, with almost 50% of the regions having no homogeneous periods with $F_{p-} = 1$. The map for F_{-} (Fig. 5b) allows for some additional considerations on the spatial distribution, with moderate maximum lengths (around 9 dekads) in most of western and central Europe, and some high values (higher than 15 dekads) in some regions of southern Europe.

In terms of temporal distribution, the histograms on Fig. 6 depict the fraction of NUTS 2 regions that includes that particular dekad in the negative homogeneous periods. Overall, the fraction values are lower than the ones observed for the positive periods (see Fig. 4), with two distinguishable peak periods in the F_{-} values, the first in early season (February-May) and the second at the end of the season (October-December).

Most of the homogeneous periods early in the season correspond to regions in western and southern Europe, and the late season periods are mostly located in central and northern Europe. In the framework of drought monitoring, the first can be potentially exploited as early warning signals of subsequent reduction in fAPAR due to drought (as seen in the positive homogenous periods), while the second mostly occur very close to the harvesting season.

3.3 Performance for a fixed time-window

A clear outcome of the previous analyses is that the length of the homogeneous periods with negative correlations is limited compared to the positive correlations, and mostly useful

https://doi.org/10.5194/nhess-2022-178
Preprint. Discussion started: 6 July 2022

for drought monitoring only early in the growing season. Therefore, we focus only on the positive correlation values for the successive analyses. The two lengths (6 and 8 months) derived from the data depicted in Fig. 4 are used as the minimum and maximum boundary values to find the local optimal period for each region (see Section 2.3).

The results of this bounded analysis of the local optimal period are shown in Fig. 7, where the starting dekad (d_i, panel a) and ending dekad (d_e, panel b) of the optimal period are depicted for every region. Fig. 7a shows a general pattern of an early start in Central Europe (i.e. February/March), and in few southern regions of the Mediterranean, and a late start (i.e. May/June) in most of southern and western Europe. This late start is of course in line with the previously observed negative correlations in February/May over the same regions. Analogously, Fig. 7b shows that the end of the optimal period occurs mostly around October/November in both southern and western Europe, and August/September in central Europe, with then mostly negative correlations in central and north Europe occurring after this period.

Given that these optimal periods have been derived based on the average r values in the 6 to 8-month period, both F_{p+} and F_+ can assume any values between 0 and 1. For this reason, we classified each region based on the combined values of these two metrics, as represented by the legend included in Fig. 8. In this map, the green areas show a good capability to reproduce the dynamic of yield deviation for the whole optimal period, with the regions in dark green having the overall best performance (over half of dekads with statistically significant r values and more than 2/3 with at least positive values). Conversely, the red regions show a poor capability of the fAPAR anomalies to capture the yield dynamic, with the dark red regions having less than 1/10 of statistically significant values (i.e. less than a month) and less than 1/3 of positive correlations during the optimal period.

Overall, slightly more than half (i.e. 55.8%) of the study regions are classified in one of the green classes, with a predominance of these regions in Mediterranean and south-eastern Europe. The rest of the study area is almost equally split between regions with average performance (yellow class, 23.3%), and poor performance (red classes, 20.9%). Among the red classes, the majority of the regions fall in the category with intermediate F_+ values ($1/3 < F_+ < 2/3$) but low statistically significance ($F_{p+} < 1/10$). Most of these regions are located in central Europe, between northern France, the United Kingdom, Germany and Poland.

Spain stands out as having particularly robust performances, even among the generally good performing Mediterranean area. While the start and end of the optimal period varies across the area (March to May, and September to November, respectively), the results are

https://doi.org/10.5194/nhess-2022-178
Preprint. Discussion started: 6 July 2022

consistently in the best class (dark green in Fig. 8). Among the Mediterranean countries, some mixed results can be observed in Italy and Greece.

3.4 Drought vs. no-drought years

The previous analyses show a noticeable difference in the capability of fAPAR anomalies to capture the full range of variability of yield anomalies across Europe, as quantified by the results on the optimal periods summarize in Fig. 8. For the same optimal periods, the number of fAPAR anomalies < -1 where cumulated for drought and no-drought years, separately, and the ratio between these two quantities is depicted in Fig. 9.

Overall, values greater than 1 are observed over most of Europe in Fig. 9, suggesting a good capability of fAPAR anomalies to detect the effects of drought on annual yield. While the ratio is only slightly higher than one in some regions where the previous analyses highlight poor performances (i.e. UK and France), effects of the main drought events on yield are still well-captured.

Finally, the plot in Fig. 10 show a comparison between the ratio computed on the optimal period (grey area) and the one computed on the full year (all 36 dekads, black area). This plot show an overall increase in the ratio when only the dekads in the optimal period are considered, which translate in a better ability to discriminate between drought and no/drought years compared to simply account for all the anomalies observed across the full year.

4. Discussion

The results reported in the previous section are based on the assumption that anomalies of cereal yields are a good proxy variable for drought impacts, as demonstrated for example by Brás et al. (2021) who quantified an approximately 9% reduction in European cereal yields due to historical droughts (1961-2018), with an increasing intensity in more recent years. The spatial patterns in negative yield anomalies used in this study, and the cross comparison with documented past drought events, confirm this general assumption.

The common element for all the performed analyses is the independent use of each dekadal fAPAR time series, since this is how data are commonly used in operational monitoring systems. While different results may be achieved by using metrics based on the full growing season (e.g. Kang et al., 2018), such analyses are not easily transferable to a near-real time monitoring framework. Overall, the correlation coefficients computed using fAPAR collected during multiple dekads suggests a predominance of positive values over all regions. This is in line with the expected direct relationship between fAPAR and yield during the core growing season, as well as with most of the past studies which focused primarily on

https://doi.org/10.5194/nhess-2022-178
Preprint. Discussion started: 6 July 2022

the positive correlation. Indeed, most of the maximum values of correlation seems to be located within the conventional growing season, and the south-north gradient observed in both of the positive homogeneous period maps (Fig. 3) is in broad agreement with the expected increasing gradient in growing season length observed over Europe (Rötzer and Chmielewski, 2001). However, while studies on satellite-derived phenology have detected growing season lengths ranging from 5 to 9 months (Rötzer and Chmielewski, 2001), the average length of the periods with positive and statistically significant correlations seems to be shorter.

Consistently high positive correlation values are obtained over most of Spain, in line with a recent study over the region (García-León et al., 2019), which reported good performances of the satellite-based Vegetation Condition Index (VCI) for different type of cereals, especially for winter wheat and barley. Over central Italy, Todisco et al. (2008) observed good correlation between yield in sunflower and sorghum with common drought indices (Standardized Precipitation Index, SPI, and Soil Moisture Severity Index), with a maximum correlation around weeks 27-29 of the growing season (i.e. July) and statistically significant values for periods ranging from 2 to 4 months. Similar timing, but with a slightly shorter optimal length, has been observed in our analysis for the same area.

For Germany, Bachmair et al. (2018) found significant correlation values between VCI and Vegetation Health Index (VHI) anomalies in the month of August, and yield deviations for maize, that are comparable with the maximum values observed for western Germany in our study. A mix of high correlation and missing data is reported in that study for eastern Germany, where our results are statistically significant only for a very limited period. These differences may be explained by the focus on specific crop types, as the same authors also highlight how their results varied for the different crops.

Similar to our results, Labudová et al. (2017) found significant correlation with SPI and Standardized Precipitation Evapotranspiration Index (SPEI) in the Danubian lowlands only for summer months, or for a very limited time (i.e. June) in the Eastern Slovak lowlands. For these regions, the values of the maximum homogeneous period with F_{p+} =1 ranged between 3 and 9 dekads as shown in Fig. 3.

The presence of limited periods with consecutive negative correlations early in the growing season may be related to the lagged response of vegetation to water deficits (Crow et al., 2012), as well as to the limited immediate effect of water deficit during energy-limited periods (Zscheischler et al., 2015). This inverse relationship is currently under-explored in drought monitoring systems, which mostly focus on the direct relationship, and it may have

https://doi.org/10.5194/nhess-2022-178
Preprint. Discussion started: 6 July 2022

an interesting role as an early warning tool under specific conditions. However, the results obtained in this study suggest a limited temporal extension and statistical robustness of the periods with inverse relationships, which usually are followed by much longer and robust periods of direct relationship.

The late start of the optimal period in many regions of the Mediterranean and western Europe, compared to the rest of the domain, is associate to the presence of these periods of inverse relationship early in the growing season. Given the particular climate of the Mediterranean region, and the key role of the dry and hot summer months in propagating the droughts in the area, a lagged response in vegetation is expected. In contrast, Central Europe is characterized by an early start of the optimal period (March to August) that seems to precede the expected growing season (June to October). For central Europe, Potopová et al. (2015) found high yield-drought correlation for cereals (better than other crops) over Czech Republic between April-June, a result in line with our findings. The late start (April/May) in the northern regions of Scandinavia compared to central Europe, is mostly explained by the lack of reliable fAPAR data earlier in the year, due to low sun angles.

Focusing on the optimal period, mixed performances are obtained in Italy, with low agreement particularly in Sardinia and regions along the Apennine mountains. Although García-León et al. (2021) found a positive relationship between annual-cumulated fAPAR anomalies and yield for most main crop types, the aggregation of the results at national scale does not allow the detection of differences among regions. Given the complex morphology of those regions, potential unreliability in the fAPAR estimates may be a possible cause for the poor performances. Complex morphology can also be the reason for poor results over few other Mediterranean areas, such as Greece.

One possible contributing factor underlying the spatial differences in the retrieved optimal periods, is the effects of different predominant cereal types that are cultivated locally. This is supported by other studies that have demonstrated different responses for different crop types (García-León et al., 2021; Labudová et al., 2017). While applying the analysis to different plant types may be useful to understand better the relationship between drought conditions and yield for each specific crop, the results of this study for all cereals provide valuable experimental information that can be more easily ingested into an operational drought monitoring system, which specializes not only in agricultural drought impacts.

https://doi.org/10.5194/nhess-2022-178
Preprint. Discussion started: 6 July 2022

5. Summary and Conclusions

In this study, records of annual crop yield data for cereals, which are collected by Eurostat, were used to evaluate the capability of satellite-derived fAPAR time series data to capture the effect of drought events on crop production for different periods of the year and growth stages of vegetation.

Overall, the analysis of the correlograms computed by plotting anomalies of dekadal fAPAR values against yearly yield deviations, was used for three main purposes:

- Investigation on continuous streaks of dekads with homogeneous behaviour (direct *vs.* inverse) and agreement (i.e. statistical significance) but with different temporal length.
- Investigation of fixed length (6 to 8 months) optimal periods, defined as function of the maximum average *r* within the given range of lengths.
- Evaluation of the capability of fAPAR anomalies during the optimal periods to discriminate between drought and no-drought years.

The analyses confirm the March to October period as the most relevant to positively correlate anomalies of fAPAR and crop yield, being the period when most of the highest values of correlation are observed, and when most of the continuous periods with statistically significant and positive *r* values are located. There is a generally good agreement comparing these findings with both the duration and temporal location of the commonly defined growing seasons in Europe. While some periods with consistent negative correlations are also observed between February and May, these are generally limited in length to be considered as primary source of information to reproduce yield dynamics, but they have potential as valuable early warning information.

The average growing period in Europe is usually characterized by a marked south-to-north gradient, which is also observed in our analysis of the 6 to 8-month optimal periods based on average *r* values. Some clear spatial patterns emerge in this analysis, such as the early start in most of central Europe and the southern Mediterranean, and the late start in southern and western Europe. While these spatial patterns do not exactly match commonly observed satellite-derived growing seasons, they provide potentially valuable information that can be incorporated into operational drought monitoring systems.

Another key output of the study is the generally good correlation between fAPAR anomalies and crop yield anomalies over most of the Mediterranean regions and across the full range of variability of yield data. Given the well documented high vulnerability of this region to drought and the increasing threat posed by climate change (Cammalleri et al., 2020;

https://doi.org/10.5194/nhess-2022-178
Preprint. Discussion started: 6 July 2022

458 Dubrovský et al., 2014), the ability to link satellite-observed fAPAR anomalies with actual
459 impacts in agriculture is a promising new development that merits further exploration.
460 This study also highlighted the overall limited correlation, outside of very short time
461 periods, between fAPAR and yield over most of the NUTS 2 regions in central Europe.
462 Further analyses may be needed to better understand the reason behind this result. In this
463 context, a recent study by Beillouin et al. (2020) has demonstrated how simple climate
464 variables (i.e. high temperature and low precipitation) can explain much of the yield
465 variability in central Europe, in contrast with the situation in southern Europe. It is important
466 to further remark that even over these regions where the overall performance is limited,
467 fAPAR anomalies are still successful in discriminating between drought and no-drought
468 conditions, which is a major requirement in drought monitoring systems.
469
470
471 **Data availability:** The fAPAR dataset used in this study can be retrieved from the JRC Data
472 catalogue (EDO, 2021).
473
474 **Author contribution:** CC designed the experiments with inputs from AT and NMC. CC
475 developed the codes and performed the analyses. CC prepared the manuscript with
476 contributions and revisions from all co-authors.
477
478 **Competing interests:** The authors declare that they have no conflict of interest.

https://doi.org/10.5194/nhess-2022-178
Preprint. Discussion started: 6 July 2022

References

Atzberger, C., Klisch, A., Mattiuzzi, M., Vuolo, F., 2014. Phenological metrics derived over the European continent from NDVI3g data and MODIS time series. Remote Sens. 6(1), 257-284. doi:10.3390/rs6010257.

Bachmair, S., Tanguy, M., Hannaford, J., Stahl, K., 2018. How well do meteorological indicators represent agricultural and forest drought across Europe? Env. Res. Letters 13, 034042. doi:10.1088/1748-9326/aaafda.

Barros, J.R.A., Guimaraes, M.J.M., Simões, W.L., de Melo, N.F., Angelotti, F., 2021. Water restriction in different phenological stages and increased temperature affect cowpea production. Agr. Sci. 45, 1-12. doi:10.1590/1413-7054202145022120.

Beillouin, D., Schauberger, B., Bastos, A., Ciais, P., Makowski, D., 2020. Impact of extreme weather conditions on European crop production in 2018. Phil. Trans. R. Soc. B 375, 20190510. doi:10.1098/rstb.2019.0510.

Bogdan, O., Marinică, I., Mic, L.-E., 2008. Characteristics of the summer drought 2007 in Romania. Proceedings of the 2008 BALWOIS Conference. 27-31 May 2008, Ohrid, Republic of Macedonia. Available at: http://balwois.com/wp-content/uploads/old_proc/ffp-1075.pdf. [last access: July 2021].

Brás, T.A., Seixas, J., Carvalhais, N., Jägermeyr, J., 2021. Severity of drought and heatwave crop losses tripled over the last five decades in Europe. Environ. Res. Lett. 16, 065012. doi:10.1088/1748-9326/abf004.

Brown, R.G., Meyer, R.F., 1961. The fundamental theory of exponential smoothing. Oper. Res. 9, 673-685. doi:10.1287/opre.9.5.673.

Buras, A., Rammig, A., Zang, C.S., 2020. Quantifying impacts of the drought 2018 on European ecosystems in comparison to 2003. Biogeosciences 17, 1655-1672. doi:10.5194/bg-17-1655-2020.

Cammalleri, C., Naumann, G., Mentaschi L., Bisselink, B., Gelati, E., de Roo, A., Feyen, L., 2020. Diverging hydrological drought traits over Europe with global warming. Hydrol. Earth Syst. Sci. 24, 5919-5935. doi:10.5194/hess-24-5919-2020.

Ceglar, A., Toreti, A., Zampieri, M., Manstretta, V., Bettati, T., Bratu, M., 2020. Clisagri: An R package for agro-climate services. Climate Serv. 20, 100197. doi:10.1016/j.cliser.2020.100197.

Chaves, M.M., Pereira, J.S., Maroco, J., Rodrigues, M.L., Ricardo, C.P.P., Osório, M.L., Carvalho, I., Faria, T., Pinheiro, C., 2002. How Plants Cope with Water Stress in the

https://doi.org/10.5194/nhess-2022-178
Preprint. Discussion started: 6 July 2022

Field? Photosynthesis and Growth. Annals Botany 89(7), 907-916. doi:10.1093/aob/mcf105.

Crow, W., Kumar, S.W., Bolten, J.D., 2012. On the utility of land surface models for agricultural drought monitoring. Hydrol. Earth Syst. Sci. 16, 34-51-3460. doi:10.5194/hess-16-3451-2012.

Demirevska, K., Zasheva, D., Dimitrov, R., Simova-Stoilova, L., Stamenova, M., Feller, U., 2009. Drought stress effects on Rubisco in wheat: changes in the Rubisco large subunit. Acta Phisiol. Plant 31, 1129-1138. doi:10.1007/s11738-009-0331-2.

Dubrovský, M., Hayes, M., Duce, P., Trnka, M., Svoboda, M., Zara, P., 2014. Multi-GCM projections of future drought and climate variability indicators for the Mediterranean region. Reg. Environ. Change 14, 1907-1919. doi:10.1007/s10113-013-0562-z.

European Drought Observatory, EDO, 2021. EDO Fraction of Absorbed Photosynthetically Active Radiation (FAPAR) Anomaly (MODIS) (version 1.3.2). European Commission, Joint Research Centre (JRC) [Dataset] PID: http://data.europa.eu/89h/91a222a0-74fe-468f-b53a-b622aa1161cf.

Eurostat, 2020. Annual crop statistics: Handbook 2020 edition. 167 pp. Available at: https://ec.europa.eu/eurostat/cache/metadata/Annexes/apro_cp_esms_an1.pdf [last access: July 2021].

Food and Agriculture Organization of the United Nations (FAO), 2015. The impact of natural hazards and disasters on agriculture and food security and nutrition: A call for action to build resilient livelihoods. Rome, Italy, 16 pp. Available at: http://www.fao.org/3/i4434e/i4434e.pdf [last access: July 2021].

Food and Agriculture Organization of the United Nations (FAO), International Fund for Agricultural Development (IFAD), United Nations Children's Fund (UNICEF), World Food Programme (WFP), World Health Organization (WHO), 2018. The State of Food Security and Nutrition in the World 2018. Building climate resilience for food security and nutrition. Rome, Italy, 202 pp. Available at: https://www.fao.org/3/I9553EN/i9553en.pdf [last access: December 2021].

García-Herrera, R., Paredes, D., Trigo, R.M., Trigo, I.F., Hernandez, H., Barriopedro, D., Mendes, M.T., 2007. The outstanding 2004-2005 drought in the Iberian Peninsula: associated atmospheric circulation. J. Hydrometeorol. 8, 483–498. doi:10.1175/JHM578.1.

https://doi.org/10.5194/nhess-2022-178
Preprint. Discussion started: 6 July 2022

García-Herrera, R., Garrido-Perez, J.M., Barriopedro, D., Ordóñez, C., Vicente-Serrano, S.M., Nieto, R., Gimeno, L., Sorí, R., Yiou, P., 2019. The European 2016/17 Drought. J. Climate 32, 3169-3187. doi:10.1175/JCLI-D-18-0331.1.

García-León, D., Contreras, S., Hunink, J., 2019. Comparison of meteorological and satellite-based indices as yield predictors of Spanish cereals. Agr. Water Manage. 213, 388-396. doi:10.1016/j.agwat.2018.10.030.

García-León, D., Standardi, G., Staccione, A., 2021. An integrated approach for the estimation of agricultural drought costs. Land Use Policy 100, 104923. doi: 10.1016/j.landusepol.2020.104923.

Kang W., Wang, T., Liu, S., 2018. The response of vegetation phenology and productivity to drought in semi-arid regions of northern China. Remote Sens. 10(5), 727. doi:10.3390/rs10050727.

Knyazikhin, Y., Martonchik, Y.V., Myneni, R.B., Diner, D.J., Running, S.W., 1998. Synergistic algorithm for estimating vegetation canopy leaf area index and fraction of absorbed photosynthetically active radiation from MODIS and MISR Data. J. Geophys. Res. 103, 32257–32274. doi:10.1029/98JD02462.

Klisch, A., Atzberger, C., 2014. Evaluating phenological metrics derived from the MODIS time series over the European continent. PFG 5, 409-421. doi:10.1127/1432-8364/2014/0233.

Labudová, L., Labuda, M., Takáč, J., 2017. Comparison of SPI and SPEI applicability for drought impact assessment on crop production in the Danubian lowland and the East Slovakian lowland. Theor. Appl. Climatol. 128, 491-506. doi:10.1007/s00704-016-1870-2.

Myneni, R.B., 2015. MOD15A2H MODIS/Terra Leaf Area Index/FPAR 8-Day L4 Global 500m SIN Grid V006. NASA EOSDIS Land Processes DAAC. doi:10.5067/modis/mod15a2h.006.

Potopová, V., Štepánek, P., Možný, M., Turoktt, L., Soukup, J., 2015. Performance of the standardized precipitation evapotranspiration index at various lags for agricultural drought risk assessment in the Czech Republic. Agric. For. Meteorol. 202, 26-38.

Rebetez, M., Mayer, H., Dupont, O., Schindler, D., Gartner, K., Kropp, J.P., Menzel, A., 2006. Heat and drought 2003 in Europe: A climate synthesis. Ann. For. Sci. 63, 569-577. doi:10.1051/forest:2006043.

Rembold, F., Meroni, M., Urbano, F., Csak, G., Kerdiles, H., Perez-Hoyos, A., Lemoine, G., Leo, O., Negre, T., 2019. ASAP: A new global early warning system to detect anomaly

https://doi.org/10.5194/nhess-2022-178
Preprint. Discussion started: 6 July 2022

hot spots of agricultural production for food security analysis. Agr. Systems 168, 247-257. doi:10.1016/j.agsy.2018.07.002.

Rojas, O., Vrieling, A., Rembold, F., 2011. Assessing drought probability for agricultural areas in Africa with coarse resolution remote sensing imagery. Remote Sens. Environ. 115, 343-352. doi: 10.1016/j.rse.2010.09.006.

Rossi, S., Weissteiner, C., Laguardia, G., Kurnik, B., Robustelli, M., Niemeyer, S., Gobron, N., 2008. Potential of MERIS fAPAR for drought detection. In: Proceedings of the 2nd MERIS/(A)ATSR User Workshop, ESA SP-666, edited by H. Lacoste and L. Ouwehand, 6. Frascati, Italy. ESA Communication production Office.

Rötzer, T., Chmielewski, F.M., 2001. Phenological maps of Europe. Climate Res. 18, 249-257. doi:10.3354/cr018249.

Sima, M., Popovici, E.-A., Bălteanu, D., Micu, D.A., Kucsicsa, G., Dragotă, C., Grigorescu, I., 2015. A farmer-based analysis of climate change adaptation options of agriculture in the Bărăgan Plain, Romania. Earth Perspect. 2, 5. doi:10.1186/s40322-015-0031-6.

Somorowska, U., 2016. Changes in drought conditions in Poland over the past 60 years evaluated by the Standardized Precipitation-Evapotranspiration Index. Acta Geophys. 64(6), 25-30-2549. doi:10.1515/acgeo-2016-0110.

Spinoni, J., Naumann, G., Vogt, J.V., Barbosa, P., 2015. The biggest drought events in Europe from 1950 to 2012. J. Hydrol. Reg. Studies 3, 509-524. doi:10.1016/j.ejrh.2015.01.001.

Stahl, K., Kohn, I., Blauhut, V., Urquijo, J., De Stefano, L., Acácio, V., Dias, S., Stagge, J.H., Tallaksen, L.M., Kampragou, E., Van Loon, A.F., Barker, L.J., Melsen, L.A., Bifulco, C., Musolino, D., de Carli, A., Massarutto, A., Assimacopoulos, D., Van Lanen, H.A.J., 2016. Impacts of European drought events: insights from an international database of text-based reports. Nat. Hazards Earth Syst. Sci. 16, 801-819. doi:10.5194/nhess-16-801-2016.

Stallmann, J., Schweiger, R., Pons, C.A.A., Müller, C., 2020. Wheat growth, applied water use efficiency and flag leaf metabolome under continuous and pulsed deficit irrigation. Sci. Rep. 10, 10112. doi:10.1038/s41598-020-66812-1.

Tadesse T., Senay, G.B., Berhan, G., Regassa, T., Beyene, S., 2015. Evaluating a satellite-based seasonal evapotranspiration product and identifying its relationship with other satellite-derived products and crop yield: a case study for Ethiopia. Int. J. Appl. Earth Obs. Geoinf. 40, 39-54. doi:10.1016/j.jag.2015.03.006.

https://doi.org/10.5194/nhess-2022-178
Preprint. Discussion started: 6 July 2022

611 Todisco, F., Vergni, L., Mannocchi, F., 2008. An evaluation of some drought indices in the
612 monitoring and prediction of agricultural drought impact in central Italy. In: Santini A.,
613 Lamaddalena N., Severino G., Palladino M. (eds.). Irrigation in Mediterranean
614 agriculture: challenges and innovation for the next decades. Bari : CIHEAM, 2008, 203-
615 211, Options Méditerranéennes: Série A, Séminaires Méditerranéens; n. 84. Available
616 at: http://om.ciheam.org/article.php?IDPDF=800967 [last access: July 2021].
617 Toreti, A., Belward, A., Perez-Dominguez, I., Naumann, G., Luterbacher, J., Cronie, O.,
618 Seguini, L., Manfron, G., Lopez-Lozano, R., Baruth, B., van den Berg, M., Dentener,
619 F., Ceglar, A., Chatzopoulos, T., Zampieri, M., 2019. The Exceptional 2018 European
620 Water Seesaw Calls for Action on Adaptation. Earth's Future 7(6), 652-663. doi:
621 10.1029/2019EF001170.
622 United Nations Office for Disaster Risk Reduction, 2021. GAR Special Report on Drought
623 2021. Geneva, 210 pp. ISBN: 9789212320274. Available at:
624 https://www.undrr.org/publication/gar-special-report-drought-2021 [last access: July
625 2021].
626 Valiukas, D., 2015. Analysis of droughts and dry periods in Lithuania. Summary of Doctoral
627 Dissertation, Vilnius University, 49 pp. Available at:
628 https://epublications.vu.lt/object/elaba:8754330 [last access: July 2021].
629 van Hateren, T.C., Chini, M., Matgen, P., Teuling, A.J., 2021. Ambiguous agricultural
630 drought: Characterising soil moisture and vegetation droughts in Europe from earth
631 observation. Remote Sens. 13(19), 1990. doi:10.3390/rs13101990.
632 Vicente-Serrano, S.M., Beguería, S., Lorenzo-Lacruz, J., Camarero, J.J., López-Moreno, J.I.,
633 Azorin-Molina, C., Revuelto, J., Morán-Tejeda, E., Sanchez-Lorenzo, A., 2012.
634 Performance of drought indices for ecological, agricultural, and hydrological
635 applications. Earth Interact. 16, 1-27. doi:10.1175/2012EI000434.1.
636 Wang, Y., Tian, Y., Zhang, Y., El-Saleous, N., Knyazikhin, Y., Vermote, E., Myneni, R.B.,
637 2001. Investigation of product accuracy as a function of input and model uncertainties:
638 Case study with SeaWiFS and MODIS LAI/FPAR algorithm. Remote Sens. Environ.
639 78, 296-311. doi:10.1016/S0034-4257(01)00225-5.
640 World Meteorological Organization (WMO) and Global Water Partnership (GWP), 2016.
641 Handbook of Drought Indicators and Indices (M. Svoboda and B.A. Fuchs). Integrated
642 Drought Management Programme (IDMP), Integrated Drought Management Tools and
643 Guidelines Series 2. Geneva, 53 pp.

https://doi.org/10.5194/nhess-2022-178
Preprint. Discussion started: 6 July 2022


Natural Hazards and Earth System Sciences
Discussions

644 Yang, J., Wu, J., Liu, L., Zhou, H., Gong, A., Han, X., Zhao, W., 2020. Response of winter
645 wheat to drought in the north China plain: spatial-temporal patterns and climate drivers.
646 Water 12, 3094. doi:10.3390/w12113094.
647 Zampieri, M., Ceglar, A., Dentener, F., Toreti, A., 2017. Wheat yield loss attributable to heat
648 waves, drought and water excess at the global, national and subnational scales. Env.
649 Res. Lett. 12(6), 064008. doi:10.1088/1748-9326/aa723b.
650 Zscheischler, J., Orth, R., Seneviratne, S.I., 2015. A submonthly database for detecting
651 changes in vegetation-atmosphere coupling. Geograph. Res. Let. 42(22), 9816-9824.
652 doi:10.1002/2015GL066563.
653

https://doi.org/10.5194/nhess-2022-178
Preprint. Discussion started: 6 July 2022

Tables

Table 1. Main European drought events between 2001 and 2018 according to the maps reported in Fig. 2, and corresponding references in the scientific literature.

Year of drought event	*Area affected*	*Reference*
2003	Central Europe	Rebetez et al. (2006)
2005	Iberia Peninsula	García-Herrera et al. (2007)
2006	North-Eastern Europe	Valiukas (2015); Somorowska (2016)
2007	Eastern Europe	Bogdan et al. (2008); Sima et al. (2015)
2012	Eastern Europe	Sima et al. (2015)
2017	Southern Europe	García-Herrera et al. (2019)
2018	Central-Northern Europe	Buras et al. (2020); Toreti et al. (2019)

https://doi.org/10.5194/nhess-2022-178
Preprint. Discussion started: 6 July 2022

Natural Hazards and Earth System Sciences
Discussions

660 **Figures**

661

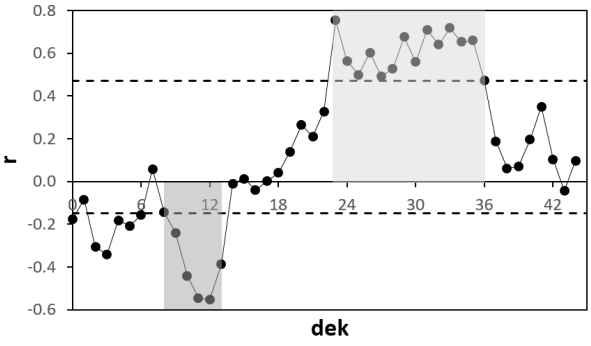

662

663 **Fig. 1.** Example of correlogram for one NUTS 2 region in Italy (ITI1, Tuscany). Each value
664 represents the Spearman correlation coefficient between the fAPAR anomaly time series of a
665 specific dekad and the yearly yield anomalies. The two horizontal dashed lines represent the
666 positive statistical significant value at p = 0.05 and the minimum negative threshold (r = -
667 0.15). Dekads are defined starting from the first dekad of October of the previous year (e.g.
668 dek = 23 refers to the last dekad of May of the current year).

669

https://doi.org/10.5194/nhess-2022-178
Preprint. Discussion started: 6 July 2022

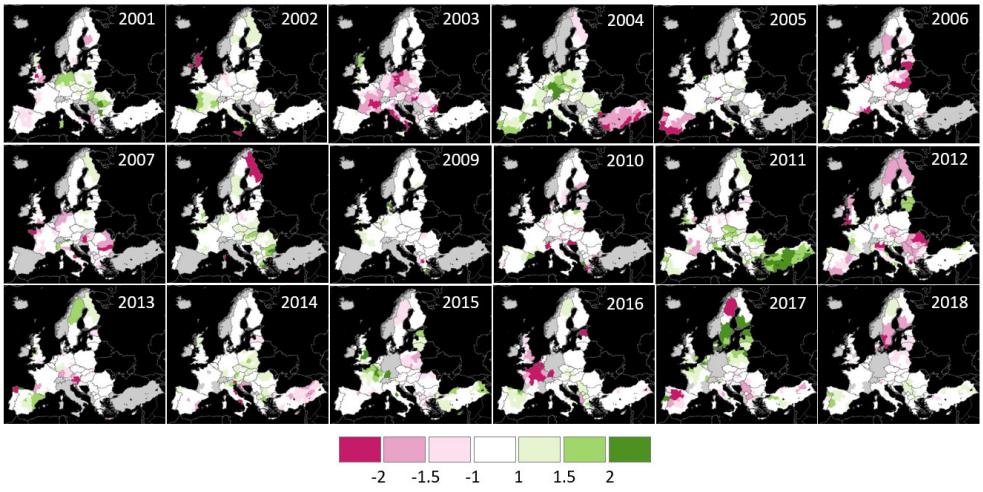

670

671 **Fig. 2.** Spatial distribution of annual standardized yield anomalies for the period 2001-2018.
672 Anomalies are mapped at NUTS 2 level, with the exception of the areas detailed in Section
673 2.1. Data in grey are missing.

674

https://doi.org/10.5194/nhess-2022-178
Preprint. Discussion started: 6 July 2022

Natural Hazards and Earth System Sciences
Discussions
Open Access
EGU

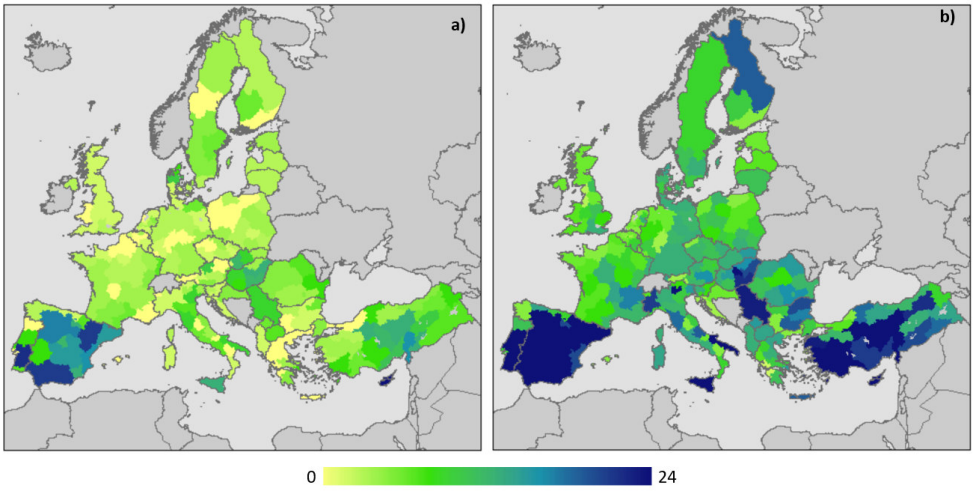

675

676 **Fig. 3.** Spatial distribution of the length (in dekads) of the longest period with $F_{p+} = 1$ (panel
677 a) and $F_{+} = 1$ (panel b).

678

https://doi.org/10.5194/nhess-2022-178
Preprint. Discussion started: 6 July 2022

Natural Hazards and Earth System Sciences
Discussions

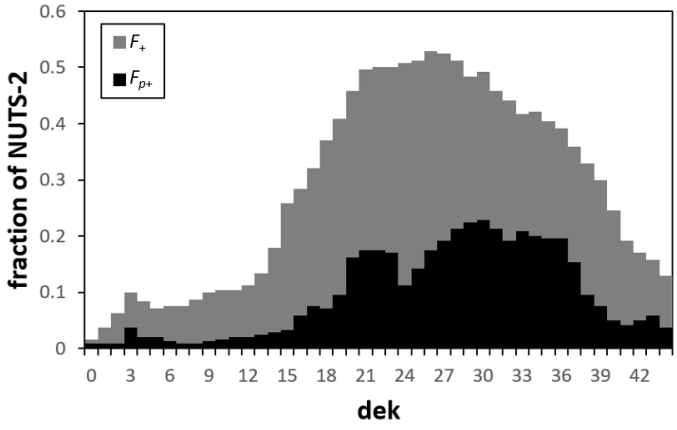

679

680 **Fig. 4.** Fraction of NUTS 2 regions for which each dekad is included in the longest
681 homogeneous period with $F_{p+} = 1$ (black) or $F_+ = 1$ (grey).

682

https://doi.org/10.5194/nhess-2022-178
Preprint. Discussion started: 6 July 2022

Natural Hazards and Earth System Sciences
Discussions
Open Access
EGU

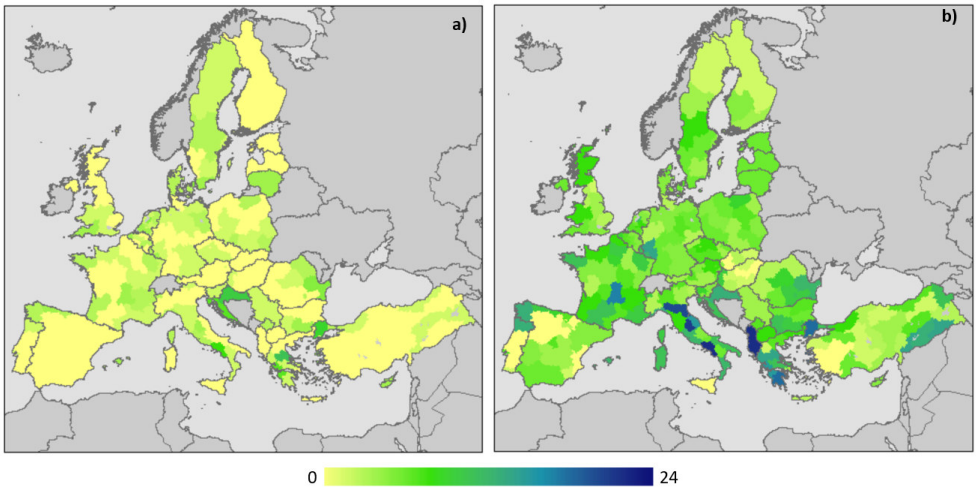

683

684 **Fig. 5.** Spatial distribution of the length (in dekads) of the longest period with $F_{p-} = 1$ (panel
685 a) and $F_{-} = 1$ (panel b).

686

https://doi.org/10.5194/nhess-2022-178
Preprint. Discussion started: 6 July 2022

Natural Hazards and Earth System Sciences
Discussions

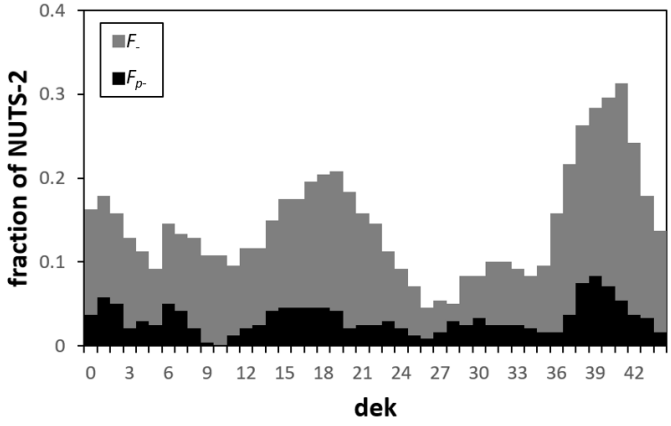

687

688 **Fig. 6.** Fraction of NUTS 2 regions for which each dekad is included in the longest
689 homogeneous period with $F_{p\text{-}} = 1$ (black) or $F_{\text{-}} = 1$ (grey).

690

https://doi.org/10.5194/nhess-2022-178
Preprint. Discussion started: 6 July 2022

Natural Hazards and Earth System Sciences
Discussions

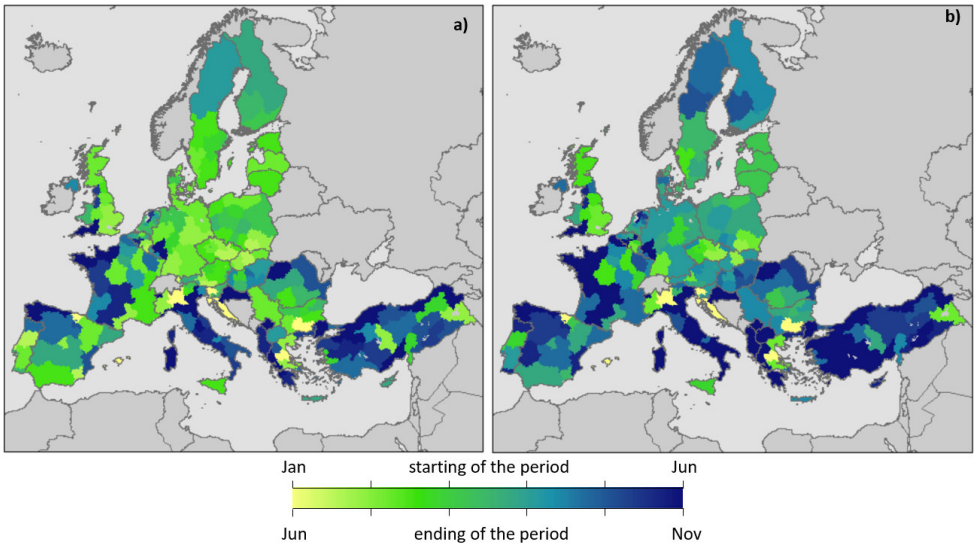

691

692 **Fig. 7.** Spatial distribution of (a) the starting dekad, and (b) the ending dekad, of the local
693 optimal period based on the average correlation and bounded by a length from 6 to 8 months.

694

https://doi.org/10.5194/nhess-2022-178
Preprint. Discussion started: 6 July 2022

Natural Hazards and Earth System Sciences
Discussions

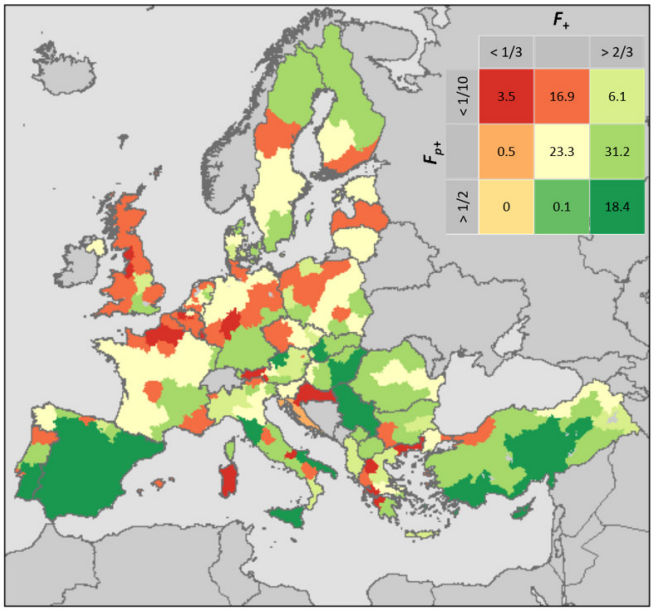

Fig. 8. Synthetic representation of the performance of dekadal fAPAR anomalies in reproducing the yearly yield variations during the local optimal period. The inserted legend shows the values of F_{p+} and F_+ for each category, with the numbers inside each square representing the percentage (%) of the total NUTS 2 regions (out of 240) that falls under each category.

https://doi.org/10.5194/nhess-2022-178
Preprint. Discussion started: 6 July 2022

Natural Hazards and Earth System Sciences
Discussions

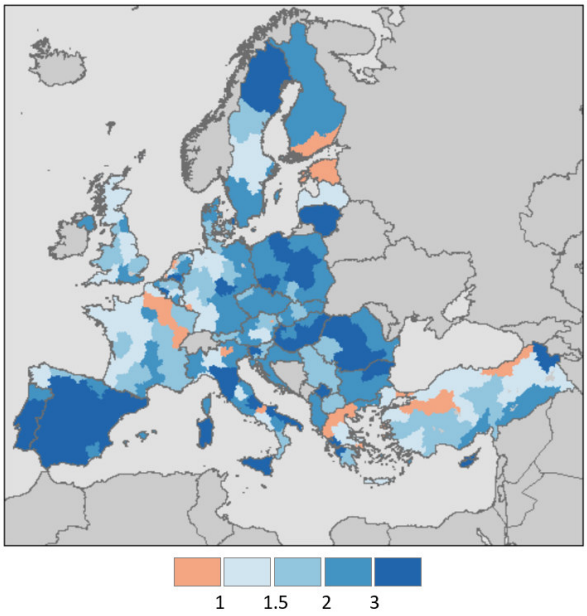

Fig. 9. Spatial distribution of the ratio between the number of fAPAR anomalies < -1 in the optimal period (see section 3.3) during drought years (yield anomalies < -1) and no-drought years (yield anomalies ≥ -1).

https://doi.org/10.5194/nhess-2022-178
Preprint. Discussion started: 6 July 2022

Natural Hazards and Earth System Sciences
Discussions

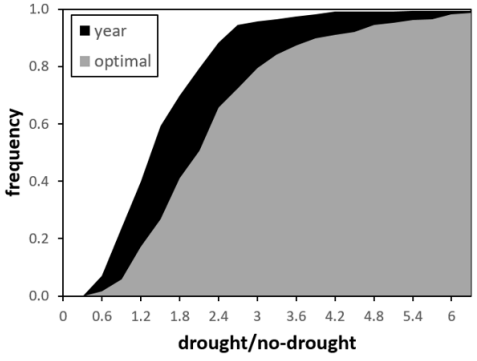

707

708 **Fig. 10.** Cumulated frequency of: i) the ratio between the number of fAPAR anomalies < -1 in
709 the optimal period (see section 3.3) during drought years (yield anomalies < -1) and no-
710 drought years (yield anomalies ≥ -1) (optimal, grey area); and ii) the ratio between the number
711 of fAPAR anomalies < -1 in the full year (36 dekads) during drought and no-drought years
712 (year, black area).